Research of line-of-sight angle on aero-optic imaging deviation for vehicles flying at 40—60 km*

XU Liang[1], ZHAO Shiwei[1], and WANG Tao[2]**

1. Tianjin Key Laboratory of Complex Control Theory and Application, School of Electronic Engineering and Automation, Tianjin University of Technology, Tianjin 300384, China

2. School of Intelligent Engineering, Sun Yat-sen University, Guangzhou 510275, China

(Received 10 July 2022; Revised 9 September 2022)

Aero-optical imaging deviation is a kind of optical effect, aiming at a conical aircraft. This paper analyzes the influence of the aircraft on the imaging deviation with the change of altitude and line-of-sight angle. In this paper, the relationships between imaging deviation and altitude as well as line-of-sight angle are analyzed, and the coupling relationship between altitude and line-of-sight angle is studied. We give the imaging deviation results of 5°—75° line-of-sight angle. The analysis shows that when the line-of-sight angle is in the range of 5°—35°, the imaging deviation is more sensitive, while the line-of-sight angle is in the range of 35°—75°, the imaging deviation is relatively flat, and the imaging deviation does not gradually decrease with the increase of line-of-sight angle, but there is a turning point in the middle of 5°—75°. The imaging deviation decreases first and then increases, and the turning point of line-of-sight angle is closely related to height.

Document code: A **Article ID:** 1673-1905(2023)04-0242-6

DOI https://doi.org/10.1007/s11801-023-2123-0

When the infrared-guided aircraft moves at high speed in the atmosphere, the gas in the head of the aircraft will be severely compressed, and a high-pressure, high-density, high-temperature turbulent flow field will be generated between the aircraft and the free flow of the atmosphere. The density of the gas in the flow field will also change randomly, so that the distribution of the refractive index of the flow field will also show non-uniformity, resulting in blur, jitter and offset of the target image, which seriously affects the accuracy of precise guidance[1-5]. Especially in military applications, these effects are often fatal.

Summarizing past domestic and foreign literatures, aero-optical effects mainly include aerodynamic thermal radiation effects and light transmission effects[6]. The aerothermal radiation effect is mainly studied on the optical head cover. In order to reduce the influence of the aero-optical effect, the researchers reduce the influence of aerodynamic heat on the window material by adding a cooling setting or non-cooling window material to the window. ZHANG et al[7] proposed to reduce the influence of thermal radiation effect by selecting the appropriate optical head cover material. DING et al[8] mentioned that the tangential jet not only has little influence on light transmission, but also has a fast-cooling rate. This paper mainly studies the optical transmission effect, that is, the influence of the change of the aero-optical flow field on the aero-optical imaging deviation. Practice has proved that infrared guided aircraft will be affected by altitude, Mach number, angle of attack and line-of-sight angle.

XU et al[9] established a two-dimensional aircraft model and proposed that the imaging deviation caused by the flow field gradually decreases with the increase of the height when the high-speed aircraft flies in the altitude range of 10—60 km. XU et al[10] changed the model from two-dimensional to three-dimensional one, and proposed that within the altitude range of 0—25 km for high-speed aircraft, the imaging deviation law is basically consistent with the results obtained previously. The research of GORDEYEV et al[11] revealed the quadratic relationship between aero-optical distortion and Mach number. YAO[12] revealed that in the range of 5°—85° line-of-sight angle, the imaging deviation decreases with increasing the line-of-sight angle.

The previous studies are all studying the influence of a certain factor change on the aero-optical imaging deviation[13-15]. Based on Ref.[12], this paper changes the two-dimensional aircraft model into a three-dimensional model and studies the altitude and line-of-sight angle together changing the effect on imaging deviation. When the height changes, the change of the line-of-sight angle to the imaging deviation is not static, but changes with the change of the height. At different altitudes, the line-of-sight angle for minimum imaging deviation is also

* This work has been supported by the National Natural Science Foundation of China (Nos.61308120 and 61975151).

** E-mail: liangx999@163.com

different. This means that the effects of height and line-of-sight angle on imaging deviation are coupled. The aircraft flies in the altitude range of 40—55 km, the smallest line-of-sight angle generally appears in the range of 60°—70°. Therefore, this paper mainly selects the line-of-sight angle within the range of 5°—75°.

As shown in Fig.1, when the aircraft moves at high speed in the atmosphere, the gas in the head of the aircraft is violently compressed, forming a gas flow field with non-uniform density and refractive index. Both the active system transmitting the beam and the passive system receiving the beam will be adversely affected by this flow field. In the active system, the flow field attenuates or deviates the energy of the projected beam from the irradiation target. In the passive system, the flow field deviation blurs and jitters the image received by the optical system. The effect of this flow field on optical propagation and optical imaging is called aero-optical effect.

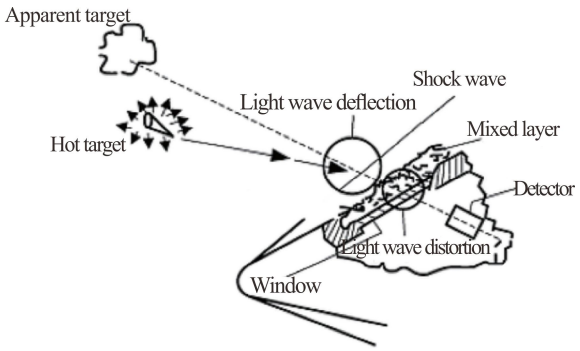

Fig.1 Schematic diagram of aero-optic effect[16]

As can be seen from the above figure, the outside of the aircraft is surrounded by a non-uniform flow field, also known as the aero-optical flow field. The outside of the aero-optical flow field is a free flow, and the light propagates in a straight line in the free flow. When the light of the target moves from the free flow to the aero-optical flow field, the light will deflect and reach the optical window on the surface of the aircraft. Because of aero-optical flow field, the position of light on the outer surface of the window will deviate from that without aero-optical flow field. This deviation is called aero imaging deviation[17].

By setting different flight conditions, different non-uniform gas flow fields can be obtained, and then different gas density and optical refractive index changes can be obtained, thus the aero-optical imaging deviation is also different. Therefore, the relationship between gas density and optical refractive index is the basis to support aerodynamic optics research, and the analysis of flow field is to analyze the changes of gas density and optical refractive index in flow field.

For inhomogeneous media with a certain space, mathematical and physical formulas can be used to describe things. Navier-stokes equations are used to describe turbulent motion in engineering applications. There are three solutions to Navier-Stokes equations, direct numerical simulation (DNS), large eddy simulation (LES) and Reynolds average method (RANS). In the study of aero-optical flow field, we mainly consider the change of average flow field caused by turbulence, which is a kind of overall and comprehensive effect. Image deviation and image blur of aero-optical effect are the result of the action of average flow field[18]. Therefore, it is natural for people to use Navier-Stokes equations, which are homogenized when solving them, to describe the flow field, namely, RANS.

The RANS is generally divided into Reynolds stress model and vortex-viscose model. The vortex-viscose model includes zero equation model, one equation model and two equation model, and the one we use most often is the k-ε two-equation model.

The compressible RANS equation for air can be written in Cartesian tensor form with summation convention.

The continuity equation is

$$\frac{\partial \rho}{\partial t}+\frac{\partial}{\partial x_i}\left(\rho u_i\right)=0. \tag{1}$$

The momentum equation is

$$\frac{\partial}{\partial t}\left(\rho u_i\right)+\frac{\partial}{\partial x_j}\left(\rho u_j u_i\right)=-\frac{\partial p}{\partial x_i}+\frac{\partial \sigma_{ij}}{\partial x_j}+\frac{\partial}{\partial x_j}\left(-\rho u_i' u_j'\right), \tag{2}$$

where u_i represents the Reynolds mean velocity y component with the mean sign omitted, ρ is density, u_i' is fluctuating velocity, and σ_{ij} is stress tensor component. Newton's law of viscosity is used to express the stress and strain rates in the constitutive relation as

$$\sigma_{ij}=\mu\left(\frac{\partial u_i}{\partial x_j}+\frac{\partial u_j}{\partial x_i}-\frac{2}{3}\delta_{ij}\frac{\partial u_k}{\partial x_k}\right), \tag{3}$$

where μ is kinetic viscosity, and δ_{ij} is the Kronecker tensor component. The last term on the right of Eq.(2) represents the gradient of the Reynolds stress. The Boussinesq vortex viscosity hypothesis was used to calculate the Reynolds stress as

$$-\rho\overline{u_i' u_j'}=\mu_{\mathrm{t}}\left(\frac{\partial u_i}{\partial x_j}+\frac{\partial u_j}{\partial x_i}\right)-\frac{2}{3}\left(\rho k+\mu_{\mathrm{t}}\frac{\partial u_k}{\partial x_k}\right)\delta_{ij}, \tag{4}$$

where μ_{t} is turbulent viscosity, and k is turbulent kinetic energy.

Zero equation model refers to using algebraic relations instead of differential equations. The model assumes that the turbulent viscosity μ_{t} is proportional to the product of the gradient of the time-averaged velocity μ_i and the mixing length l_{m}.

$$\mu_{\mathrm{t}}=l_{\mathrm{m}}^2\left|\frac{\partial u}{\partial y}\right|. \tag{5}$$

In order to make up for the limitation of the mixed length assumption of zero equation model, based on the time-averaged continuity equation and Reynolds equation of turbulent flow, the transport equation of turbulent kinetic energy k is established, and μ_{t} is expressed as the equation of k, so that the equation system is closed as

$$\frac{\partial(\rho k)}{\partial t}+\frac{\partial\left(\rho k u_i\right)}{\partial x_i}=\frac{\partial}{\partial x_j}\left[\left(\mu+\frac{\mu_i}{\sigma_k}\right)\frac{\partial k}{\partial x_j}\right]+$$

$$\mu_i\left(\frac{\partial u_i}{\partial x_j}+\frac{\partial u_j}{\partial x_i}\right)\frac{\partial u_i}{\partial x_j}-\rho C_{\mathrm{D}}\frac{k^{3/2}}{l}. \quad (6)$$

The k-ε two-equation model is the most widely used in practical engineering calculations. The governing equation of turbulence includes the equation of turbulent kinetic energy k and the equation of dissipation rate ε. The expression of the transport equation corresponding to the turbulent kinetic energy k and dissipation rate ε is

$$\frac{\partial(\rho k)}{\partial t}+\frac{\partial\left(\rho k u_i\right)}{\partial x_i}=\frac{\partial}{\partial x_j}\left[\left(\mu+\frac{\mu_{\mathrm{t}}}{\sigma_k}\right)\frac{\partial k}{\partial x_j}\right]+G_k-\rho\varepsilon, \quad (7)$$

$$\frac{\partial(\rho\varepsilon)}{\partial t}+\frac{\partial\left(\rho\varepsilon u_i\right)}{\partial x_i}=\frac{\partial}{\partial x_j}\left[\left(\mu+\frac{\mu_{\mathrm{t}}}{\sigma_\varepsilon}\right)\frac{\partial \varepsilon}{\partial x_j}\right]+$$

$$\rho C_1 E\varepsilon-\rho C_2\frac{\varepsilon^2}{k+\sqrt{\nu\varepsilon}}, \quad (8)$$

where C_1 and C_2 are empirical constants, G_k is the turbulent kinetic energy k generation term caused by average velocity gradient, and σ_k and σ_ε are the Prandtl numbers corresponding to the turbulent kinetic energy k and dissipation rate ε, respectively.

First, we need to use GAMBIT software to do geometric modeling and meshing of taper aircraft, and then call the RANS solver in FLUENT software package to do a lot of computational fluid dynamics (CFD) calculations. The CFD calculation results are imported into CFD-post software to obtain the density analysis diagram of the flow field. The gas density is converted into refractive index and imaging offset by visual studio software[19]. After the pre-processing of the aircraft, the aircraft modeling is imported into FLUENT for calculation. After the calculation, the flow field density data generated by FLUENT is imported into CFD-post to export the density data. The main parameters we change in FLUENT are the altitude, Mach number, angle of attack and line-of-sight of the aircraft.

From the average flow field density distribution at the heights of 40 km, 45 km, 50 km and 55k m, it can be seen that the flow field density diagrams at different flight altitudes are similar. The flow field density at the head of the aircraft is relatively large, while the surface flow field density of the aircraft is relatively small. In the case of constant Mach number and angle of attack, the flow field density decreases with the increase of aircraft height. As can be seen from the above figure, the maximum flow field density is 1.441×10^2, 6.998×10^3, 3.579×10^3 and 1.992×10^3, respectively. The minimum flow field density is 2.085×10^3, 7.947×10^4, 3.571×10^4 and 1.923×10^4, respectively.

Because the flight of the aircraft has different states, the imaging system of the aircraft will receive the target reflected light of different paths, resulting in different aerodynamic imaging deviations. This paper studies that when the target line-of-sight angle (the angle between the light and the aircraft axis) is different, the propagation path of the light reflected by the target in the aero-optical flow field is different, so the aerodynamic imaging deviation is also different. The range of line-of-sight angle studied in this paper is 5°—75°, and the concept of imaging deviation rate is introduced. Imaging deviation rate is defined as the small change of imaging deviation divided by the small change of related variables, which reflects the sensitivity of imaging deviation to related variables.

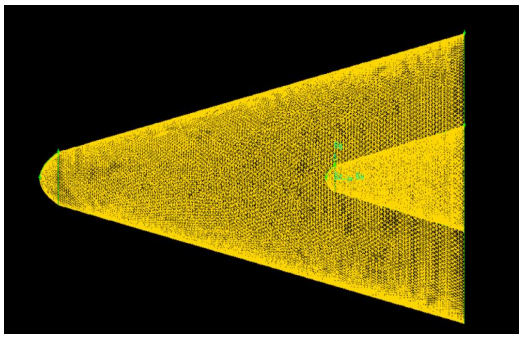

Fig.2 Grid distribution of conical aircraft

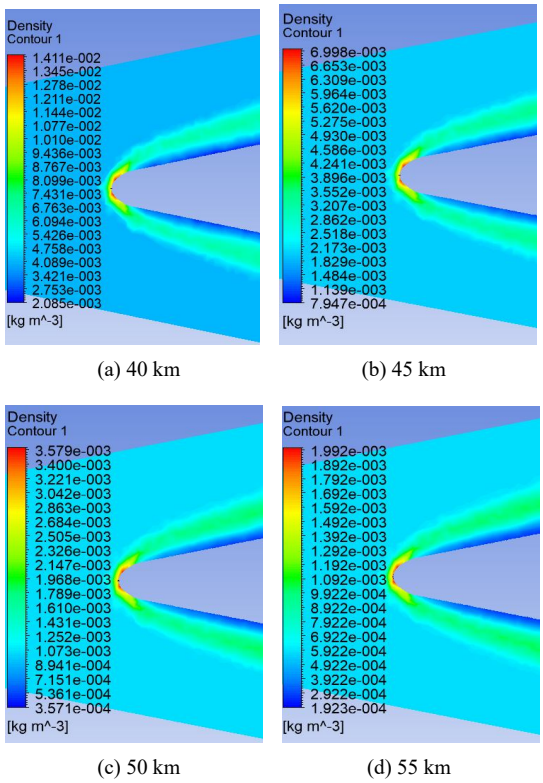

(a) 40 km (b) 45 km

(c) 50 km (d) 55 km

Fig.3 Calculation results of flow density at different altitudes (Mach is 5, and angle of attack is 0°)

In this paper, the imaging deviation rate is calculated by finite difference method. Take d as the imaging deviation, Δx as the step size of the correlation variable, and Δd as the imaging deviation rate of the correlation

variable. The central difference format is[20]

$$\nabla d = \frac{d_{i+1} - d_{i-1}}{2\Delta x}. \tag{9}$$

For the left boundary of the sequence, the first-order forward difference scheme is adopted

$$\nabla d = \frac{d_{i+1} - d_i}{\Delta x}. \tag{10}$$

For the right boundary of the sequence, the first-order forward difference scheme is adopted

$$\nabla d = \frac{d_i - d_{i-1}}{\Delta x}. \tag{11}$$

In this paper, the imaging deviation of the aircraft in the line-of-sight angle range of 5°—75° is calculated. The following results are mainly taken from the altitude of 40 km to 55 km, Mach number of Mach 5 and angle of attack of 0°.

According to the data in the above figure, the data in the table are plotted and analyzed by Origin software, the height is changed, the Mach number is fixed at Mach 5, the angle of attack is fixed at 0°, the horizontal axis is the range of line-of-sight angle, and the vertical axis is imaging offset. Then the imaging offset rate proposed above is introduced into the figure, and the influence of the change of height and line-of-sight angle on aerodynamic imaging offset is analyzed in cooperation with the figure according to the data in the table.

Use Origin software to draw the imaging deviation and imaging deviation slope diagrams for the imaging deviation data in Tab.1.

Tab.1 Aircraft condition

Altitude	Mach	Angle of attack (°)	Line-of-sight angle (°)	Imaging deviation
40	5	0	75	9.88×10^{14}
40	5	0	70	3.28×10^{14}
40	5	0	65	3.68×10^{14}
40	5	0	60	6.19×10^{14}
40	5	0	55	8.12×10^{14}
			…	
40	5	0	10	3.19×10^{6}
40	5	0	5	2.01×10^{5}
45	5	0	75	7.18×10^{14}
45	5	0	70	1.66×10^{14}
45	5	0	65	2.34×10^{14}
45	5	0	60	3.38×10^{14}
45	5	0	55	4.73×10^{14}
			…	
45	5	0	10	1.49×10^{6}
45	5	0	5	9.46×10^{6}
50	5	0	75	5.33×10^{14}
50	5	0	70	8.51×10^{15}
50	5	0	65	1.24×10^{14}
50	5	0	60	1.99×10^{14}
50	5	0	55	3.24×10^{14}
			…	
50	5	0	10	6.11×10^{7}
50	5	0	5	4.35×10^{6}
55	5	0	75	2.89×10^{14}
55	5	0	70	1.61×10^{14}
55	5	0	65	1.19×10^{14}
55	5	0	60	9.37×10^{15}
55	5	0	55	2.77×10^{14}
			…	
55	5	0	10	3.48×10^{7}
55	5	0	5	2.52×10^{6}

As can be seen from Fig.4 to Fig.7, when the line-of-sight angle is in the range of 5°—35°, the change of imaging offset rate is obvious and the imaging offset is large, while when the line-of-sight angle is in the range of 35°—75°, the change of imaging deviation rate is relatively flat and the imaging offset is relatively small.

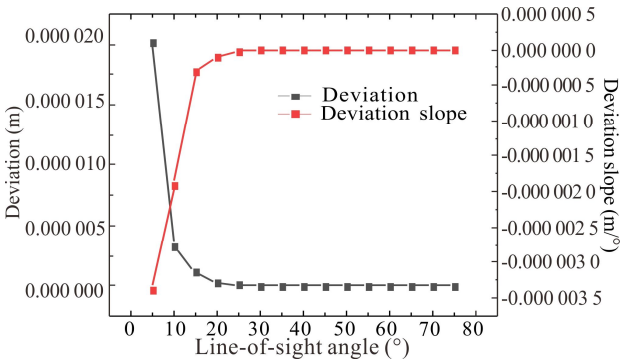

Fig.4 Effect of line-of-sight angle on imaging deviation under 40-5-0 flight condition

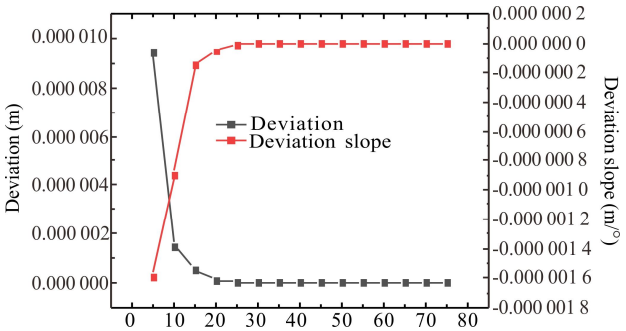

Fig.5 Effect of line-of-sight angle on imaging deviation under 45-5-0 flight condition

From Fig.4 to Fig.7 and in combination with Tab.1, it can be seen that the imaging offset decreases gradually with the increase of height, which is consistent with the law mentioned above that the non-uniform flow field density decreases gradually with the increase of height, that is, the decrease of flow field density will cause the imaging offset to decrease gradually with the increase of

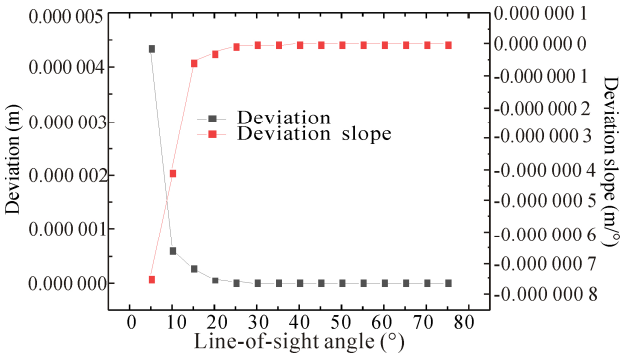

Fig.6 Effect of line-of-sight angle on imaging deviation under 50-5-0 flight condition

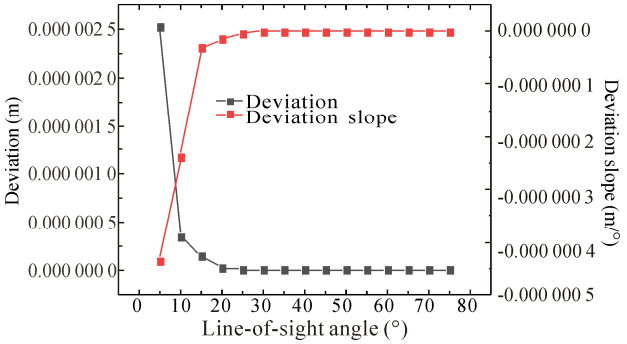

Fig.7 Effect of line-of-sight angle on imaging deviation under 55-5-0 flight condition

height. Moreover, the imaging offset does not gradually decrease with the increase of line-of-sight angle, but there is a turning line-of-sight angle, so that the change of imaging offset decreases first and then increases.

When the line-of-sight angle is in the range of 5°—35°, the imaging deviation changes greatly, while when the line-of-sight angle is in the range of 35°—75°, the imaging deviation changes little. With the increase of line-of-sight angle, the imaging deviation decreases, which means that the flow field density of light propagation will become sparse.

The curve of imaging deviation rate also has the same trend. With the increase of line-of-sight angle, the curve of imaging deviation rate approaches 0 from negative value. When the line-of-sight angle is in the range of 5°—35°, the change of imaging deviation rate is obvious, which means that the change of small line-of-sight angle is more sensitive to the change of imaging deviation, while when the line-of-sight angle is in the range of 35°—75°, the change of imaging deviation rate is relatively flat, which means that the change of large line-of-sight angle has no great impact on imaging deviation.

With the increase of height, the imaging deviation decreases gradually, which is consistent with the law mentioned above that the density of non-uniform flow field decreases gradually with the increase of altitude.

Because the large line-of-sight angle is not obvious in the above figure, but it can be seen from Tab.1 that the imaging deviation does not gradually decrease with the increase of line-of-sight angle, but there is a turning line-of-sight angle point, so that the change of imaging deviation decreases first and then increases. Under the flight conditions of 40 km and 45 km altitude, the line-of-sight angle decreases gradually from 5°—70° and increases gradually from 70°—75°. Under the flight condition of 50 km altitude, the turning line-of-sight angle is 65°, and under the flight condition of 55 km altitude, the turning line-of-sight angle is 60°, which indicates that the turning line-of-sight angle decreases with the increase of altitude.

Statements and Declarations

The authors declare that there are no conflicts of interest related to this article.

References

[1] TROMEUR E, GARNIER E, SAGAUT P. Large-eddy simulation of aero-optical effects in a spatially developing turbulent boundary layer[J]. Journal of turbulence, 2006, 7(1): N1.

[2] LI G C. Aero-optics[M]. Beijing: National Defense Industry Press, 2006.

[3] YING X L. A new branch of modern optics-aerodynamic optics[J]. China engineering science, 2005, 7(12): 1-6.

[4] LIU J, WU X Y, CHEN S C. Development analysis of typical infrared precision-guided weapons[J]. Journal of projectiles, rockets, missiles and guidance, 2022, 42(01): 19-27.

[5] XING Z, CHEN X Y, PENG Z Y. Research progress and thinking of infrared aero-optical effects (invited)[J]. Infrared and laser engineering, 2022, 51(04): 108-124.

[6] ZHANG L Q, FEI J D. Study on aero-optical effects of imaging detection for high-speed aircraft[J]. Infrared and laser engineering, 2020, 49(06): 228-232.

[7] ZHANG Q P. Research on the suppression method of aero-optical effect of beam expander system[D]. Beijing: University of Chinese Academy of Sciences, 2021. (in Chinese)

[8] DING H L, YI S H. Research progress on aero-optical effects of high-speed optical head cover[J]. Gas physics, 2020, 5(03): 1-29.

[9] XU L, CAI Y L. Influence of altitude on aero-optic imaging deviation[J]. Applied optics, 2011, 50(18): 2949-2957.

[10] XU L, ZHANG Z Z, WANG T, et al. Numerical study on aero-optical imaging deviations of vehicles at different altitudes[J]. Optoelectronics letters, 2022, 18(02): 97-102.

[11] GORDEYEV S, JUMPER E. Fluid dynamics and aero-optics of turrets[J]. Progress in aerospace science, 2010, 46(08): 388-400.

[12] YAO Y. Analysis and prediction of aero-optical imaging deviation for typical aircraft[D]. Tianjin : Tianjin

University of Technology, 2020. (in Chinese)
[13] XU L, CAI Y L. Aero-optical engineering calculation[M]. Beijing：Science Press, 2021. (in Chinese)
[14] XU L, CAI Y L. Imaging deviation through non-uniform flow fields around high-speed flying vehicles[J]. Optik, 2012, (13)：1177-1182.
[15] WANG T, ZHAO Y, XU D, et al. Numerical study of evaluating the optical quality of supersonic flow fields[J]. Applied optics, 2007, 45(23)：5545-5551.
[16] SUN X W, LIU W. Research progress of aero-optical effect[J]. Advances in mechanics, 2020, 50：250-309.
[17] XU L, CAI Y L. Influence of non-uniform flow fields on imaging deviation of side-window airborne optical systems[C]//Proceedings of IEEE International Conference on Imaging Systems and Techniques, May 17-18, 2011, Batu Ferringhi, Malaysia. New York：IEEE, 2011：12-15.
[18] XU L. Aerodynamic optical effect of infrared guided aircratf[D]. Xi'an：Xi'an Jiaotong Univerisity, 2012. (in Chinese)
[19] HAN Z Z, WANG J, LAN X P. Example and application of fluid engineering simulation[M]. Beijing：Beijing Institute of Technology Press, 2004. (in Chinese)
[20] CHEN X. Aero-optics imaging deviation and prediction with different line-of-sight roll angles[D]. Tianjin：Tianjin University of Technology, 2021. (in Chinese)